SUPERHYDROPHOBIC SURFACES WITH DOUBLE ROUGHNESS IN NANOSCALE PROMOTING CONTINUOUS DROPWISE CONDENSATION

Vandadi A.[1] and Cheng J.-T.[2,*]
[1]Department of Mechanical and Energy Engineering,
University of North Texas,
Denton, TX 76207,
USA

[2]Department of Mechanical Engineering,
Virginia Polytechnic Institute and State University,
Blacksburg, VA 24061,
USA
*Email: chengjt@vt.edu

ABSTRACT
Micro/nano-structured superhydrophobic surfaces can enhance dropwise condensation via coalescence-induced condensate jumping in well-tailored supersaturation conditions. In this paper we report our energy-based analysis of growth dynamics of dropwise condensates on biomimetic surfaces with two-tier micro/nano-textures, which are superior to flat or solely nanotextured surfaces in controlling nucleation density. To understand the role of condensate state transition, i.e., from partially wetting state (PW) to non-wetting Cassie state, in enhancing condensation heat transfer, we considered adhesion energy, viscous dissipation and contact line dissipation as the main portion of resistant energy that needs to be overcome by the condensate droplets formed in surface cavities. By minimizing the energy barrier of the state transition, we optimized first tier roughness on the hierarchically textured surfaces allowing condensates to grow preferentially in the out-of-plane direction. From the molecular kinetic (MKT) point of view, the period of the second tier roughness should be formed in excess of tens of nanometers in order to mitigate contact line dissipation. Our resistant energy study indicates that scaling down surface roughness of each tier to submicron scale or even to nanoscale can significantly facilitate the PW-Cassie transition and expedite self-propelled condensate removal.

INTRODUCTION
During vapor dropwise condensation on a superhydrophobic surface with micro/nanostructures, condensate droplets can grow and form in three morphologies, i.e., the Cassie state[1], the Wenzel state[2], or the partially wetting state (PW).[3] A condensate droplet in the Cassie state (Cassie droplet), sits on the tips of micro/nanostructures with an air layer filling the structures under the droplet. A Cassie droplet exhibits a large contact angle (> 150º) and a small hysteresis (< 5º) leading to self-propelled rapid removal via coalescence-induced jumping. Consequently Cassie condensates are desired in order to achieve self-purging of the condenser surface. On the contrary, a droplet in the Wenzel state, which is separated by a local energy barrier[4, 5] from the Cassie state, fills the structures under the droplet resulting in an immobile droplet due to strong adhesion to the structured surface. By contrast, a droplet in the PW state only partially fills the structures under the droplet. Importantly, recent studies based on droplet morphology analysis have found that condensates in the PW state on structured surfaces can give rise to 56% higher heat transfer than those on flat hydrophobic surfaces, whereas Cassie condensates counterintuitively result in 71% degradation in heat transfer because of the low thermal conductivity of the air layer underneath.[3] Therefore, PW condensates are preferred to enhance condensation heat transfer and subsequent self-propelled or coalescence-induced PW-Cassie state transition[6,7] is desired for self-purging of the condenser surface, which is essential for sustaining continuous dropwise condensation (CDC) with enhanced heat transfer.

Superhydrophobic lotus-leaf-like surfaces can not only allow for easy droplet removal at micrometric length scales during condensation but also promise to enhance heat transfer performance if designed properly. Recently droplet jumping condensation on a nanostructured superhydrophobic CuO surface has been demonstrated to enable about 30% heat transfer enhancement compared to state-of-the-art dropwise condensation.[7] However, these condensation experiments were conducted in carefully-tailored and mild thermal conditions with a low supersaturation (< 1.12) and a low critical heat flux (< 8W/cm^{2}), above which condensate flooding on the condenser surface would occur giving rise to unacceptable rise of thermal resistance therein. Therefore nano-engineered surfaces for enhanced and sustained dropwise condensation require careful control of surface structure length scale and geometry, nucleation density, droplet morphology, and even departure dynamics.

Based on interfacial energy analysis, Rykaczewski et al. reported that the growth mechanism of individual water microdroplets on nanotextured surfaces is universal and independent of the surface architecture.[8] The key role of the nanoscale topography is confinement of the base area of forming droplets, which allows droplets to grow only through contact angle increase. The nearly spherical droplets formed in this fashion become highly mobile after coalescence.

By comparing experimentally observed drop growth with interface free energy calculations, they found that the minimum

observed confined microdroplet base diameter depends directly on the nanoscale surface roughness and degree of interfacial wetting. Specifically, the microscale condensation mechanism depends on the height of a liquid film with volume equal to the fill volume between the nanostructures. Through observing condensation on one tier (layer) of nanowires in an environmental scanning electron microscope (ESEM), Rykaczewski et al. claimed that the formation of condensate nuclei (embryos) could be controlled close to the top of the nanostructures.[8] But how to form discrete condensate distribution on the surface of nanowires postponing flooding as well as validation of condensation heat transfer enhancement were not systematically studied in this work.

NOMENCLATURE

r	m	Surface roughness / Radius
b	m	First-tier width
h	m	First-tier height / latent heat
l	m	First-tier pitch size
f		Solid fraction
G	J	Activation free energy
T	K	Temperature
W	J	Work
A	m^2	Area
F	N	Force
E	J	Energy
t	s	Time
U	m/s	Velocity
Oh		Ohnesorge number
P	N/m^2	Pressure
m	kg	mass
k	Hz	Molecular displacement frequency
R		Radial coordinate
k_B	m^{2}kg/ s^{2}K	Boltzman constant
N_s	1/ m^2	Nucleation site density

Special character

ρ	kg/m^3	Density of liquid
μ	N·s/m^2	Viscous dissipation coefficient
σ	N/m	Surface tension
Ω	m^3	Tail volume
θ		Young's contact angle / Azimuthal coordinate
ζ	kg/m·s	Contact line friction
v	m^3/kg	Specific volume
Φ	N/m^2·s	Dissipation function
λ		Mean displacement

Subscripts

c	Cassie State / Cavity
w	Wenzel state / Wall
f	First-tier
n	Nano/second-tier
e	Equilibrium
l	Liquid
v	Vapor
adh	Adhesion
vis	Viscous
sat	Saturation
b	Base
lv	Liquid-vapor
sv	Solid-vapor
sl	Solid-liquid
d	Dynamic
0	Static
A	Advancing

Wang et al. put forward a wetting criterion to approximately predict condensate morphology by comparing the surface free energies of the non-equilibrium advancing Cassie and Wenzel states with a dimensionless energy ratio:[9]

$$E^* = \frac{cos\theta_{A,c}}{cos\theta_{A,w}} = \frac{-1}{rcos\theta_A} \qquad (1)$$

The essence of this equation is the critical contact angle demarcating the equilibrium Wenzel regime and the equilibrium Cassie regime[10] but herein applied on the advancing zone of an emerging condensate. Nevertheless the fundamental principles of forming droplet morphology and physical mechanisms governing its evolution process could not be reflected by this equation. Therefore, their optimization of structured surfaces based on Eq. 1 is not sufficient or not accurate to a satisfying level.

Up to date, the rationale for designing an ideal micro/nanostructured condenser surface as well as heat transfer experiments demonstrating the advantage of condensate jumping behavior in real thermal conditions are lacking. Although various such surfaces have been reported,[3-10] their development has been fortuitous, not driven by an understanding of the underlying thermal and physical processes. In particular, the dynamic growth of dropwise condensate based on laws of fluid mechanics has been rather tersely discussed in these work. In order to achieve sustained dropwise condensation with enhanced heat transfer on an engineered condenser surface, it is imperative to understand nucleation site/density distribution, the dynamic growth of condensate droplets and evolution of droplet morphology.[3] In this paper we report our energy-based analysis of growth dynamics of dropwise condensates on biomimetic surfaces with two-tier micro/nano-textures and their structural optimization.

CONDENSATE GROWTH ON SUPERHYDROPHOBIC SURFACES WITH TWO-TIER STRUCTURES

In our dropwise condensation studies we fabricated biomimetic lotus-leaf-like surfaces with two-tier hierarchical structures as shown in Figures 1(a) and 1(b), which can effectively reduce and control nucleation density as observed in ESEM.[11] The first tier consists chiefly of regularly-positioned silicon micropillars[11-15] that were subsequently coated by the second tier carbon nanotubes (CNTs). The solid fraction of the first tier pillars f_f is b^2/l^2 and the second tier has a solid fraction of f_n, so the solid fraction of the multiscale textures is $f = f_n f_f << 1$. Herein the second tier nanostructures play an important role in enhancing hydrophobicity to superhydrophobicity.[10] This type of artificially structured surface with dual-scale roughness provide a unique platform for us to study (1) energy barriers encountered by the growing condensate droplet in a unit cell, i.e., the cavity volume surrounded by micropillars, and (2) nucleation density, which has a strong correlation with the surface roughness, as well as condensate droplet interactions. In an ESEM we have observed that condensate nuclei initiated almost everywhere but preferentially grew on the nanotextures in the first tier cavities between the micropillars.[11] Each as-formed microdroplet would continue growing till eventually fill the unit cell. It has been pointed out that during the dynamic condensation process, condensed droplets are usually not in a thermodynamically equilibrium state.[3] Therefore, either

morphing-induced Laplace pressure gradient or coalescence with neighbouring condensate droplets can make the microdroplets elevate in the cavities and finally sit on top of the micropillars, i.e., the so-called PW-Cassie transition, or lead to the jumping behaviour owing to the released surface energy.[12] Here, we followed the conventional definition of the Wenzel-Cassie transition even though the terms of Wenzel state and Cassie state[1,2] were originally put forward for describing liquid droplets in an equilibrium state.
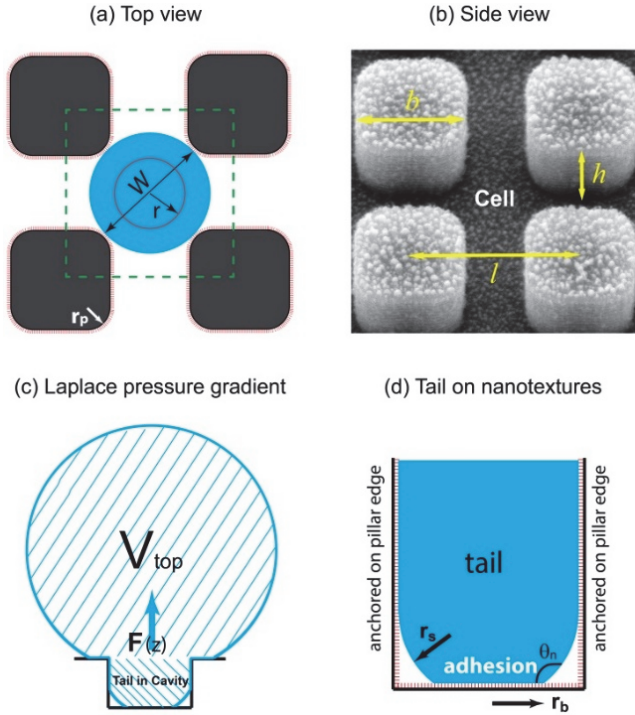

Figure 1 Top view (a) and side view (b) of the first tier pillar array on a two-tier micro/nano-textured surface. The condensate droplet anchored in the form of line contact on the vertical corner edges of the four surrounding first tier pillars in the cavity cell. (c) Side view of a condensate droplet in PW state, the desired state enhancing heat transfer. Out-of-plane movement of the condensate tail in the cavity cell is intrinsically driven by Laplace pressure gradient. (d) The base of the tail is adhered to the nanotextures in the valley (surface contact) while the tail body is in line contact with the nanotextures along first tier vertical edges. Droplet portion above pillars is not shown for the purpose of simplicity. The second tier nanotextures are shown in red in the top view (a) and cross sectional view (d).

A close inspection of condensation process in ESEM revealed the ubiquitous adhesion of condensate droplets to the second tier nanostructures in the first tier pillar valleys (Figure 2). The adhesion energy is one of the main barriers impeding the PW-Cassie transition as discussed in previous studies.[16] Besides Laplace pressure force, coalescence of droplets has been recently realized as the intrinsic driving force that can overcome the local energy barriers during condensation on textured surfaces.[12] However, viscous dissipation plays an important role in

condensate growth and can sometimes give rise to immobile coalescence[12,17] when the released surface energy in coalescence is smaller compared to viscous dissipation consumption.

In order to delay condensate flooding and achieve CDC, we aim to optimize two-tier multiscale structures by minimizing the local energy barriers. A lower energy barrier would enable condensate droplets in reduced size scale to accomplish the PW-Cassie transition and therefore an enhanced heat transfer is expected. In this paper we report our optimization of two-tier engineered surfaces by analyzing condensate growth dynamics in a unit cell confined by the first tier pillars as shown in Figure 1.
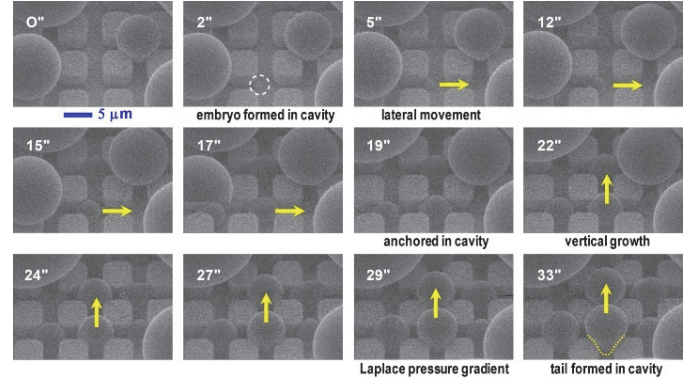

Figure 2 ESEM snapshots of dynamic growth of condensate droplets in the first tier pillar cavities on the hierarchical superhydrophobic surface ($b = 5$ μm, $h = 6$ μm, $l = 9$ μm, and 5 torr vapor pressure in ESEM). Dotted line in 33″ snapshot indicates the tail of a condensate droplet formed in PW state within four neighboring pillars.

ENERGY ANALYSIS OF GROWING CONDENSATE DROPLETS

MULTISCALE STRUCTURES FOR CONTROLLING NUCLEATION SITE DENSITY

Our study of surface roughness optimization starts with the two-tier hierarchical structures as mentioned above. In view of the nature of condensation, the formation of nucleation embryos in nanostructure cavities and in the pillar cavities (i.e., in the Wenzel state or the PW state) is ubiquitous since the critical nucleation radius of water is around tens of nanometer. The free energy barrier to nucleation in the cavity of roughness could be calculated as: [18,19]

$$\Delta G = (2 - 3\cos\theta + \cos^3\theta)[\frac{1}{3}\pi r_e^2 \sigma \qquad (2)$$
$$- \pi\sigma(r_c - r_e)^2]$$

where $r_e = 2v_l\sigma T_w/h_{lv}(T_{sat}(P_v) - T_w)$ is the equilibrium radius. The equilibrium radius of droplet in our ESEM experiments is approximately 10 nm.[11] Therefore the free energy barriers in the cavities of microstructure (4-5 μm pitch) and nanostructure (~100 nm pitch) are -1.88x10^{-11} J and -5.57x10^{-15} J, respectively. Consequently the condensate droplets are more likely to be formed in the cavities of first tier pillars, which leads to the desired PW state for heat transfer enhancement.[3] By meticulously defining roughness geometry and length scale,

engineered surfaces with multiscale structures provide an ideal platform to form discretely distributed condensates and thus can efficiently control nucleation site density.

To minimize the liquid-vapor interface (hence surface energy), nucleation embryos are preferentially initiated and formed at the bottom of the first tier pillar cavities[4] as indicated by the white dotted circle in the 2″ time frame of Figure 2. Subsequently Laplace pressure works as the driving force to laterally (in plane) propel the condensate embryos among the pillars (frames 5″ to frames 17″), during which the continuously growing condensates eventually take the shape of sphere (droplet) to maintain a relatively lower surface energy.[4] Droplet in-plane movement continues until it reaches the cavity (cell) centre and gets anchored by four surrounding pillars (frame 19″). Ideally it starts to grow upward in the out-of-plane direction instead of in-plane lateral spreading (frames 22″ to 29″) and will eventually reach the pillar top and evolve over them. Thereby a condensate tail is formed in the cavity and the condensate droplet gets entrapped in the PW state (frame 33″), which needs to be elevated to form a Cassie droplet for self-removal.

OPTIMIZATION OF SURFACE ROUGHNESS BY RESISTANT ENERGY ANALYSIS

Bahadur and Garimella studied electrowetting on dielectric (EWOD)-controlled Cassie-Wenzel transition of water droplets on artificially microstructured surfaces.[20,21] They claimed that the existence of an energy barrier for the Wenzel-Cassie reverse transition and the roughness-dependent nonconservative dissipative forces that comprise contact-line friction, contact-line pinning, and shear resistance to fluid motion inside the microstructured surface are the major factors preventing reversibility of the Cassie-Wenzel transition upon removal of the EWOD voltage and therefore dissipative forces need to be minimized to enable the complete reverse transition. In order to optimize the multiscale surface structures, the energy barriers resisting the tail transition should be minimized accordingly. The resistant energy of condensate state transition in our analysis contains three main parts: one is the adhesion energy due to the adhesion of the tail base to the nanotextures in the first tier pillar cavity (Figure 1d), the second is the subsequent viscous dissipation during the elevation of the tail from the cavity to the pillar tips, and the third is related to contact line dissipation that occurs within the three phase contact zone.

In view of the intricacy of the PW-Cassie transition and the excessive factors affecting the dynamic process we applied scaling laws in our analysis to address the main factors and attributions. The crucial step to form a mobile Cassie droplet is to first detach the tail from the cavity base and subsequently to expel the tail to the top of the pillars (PW to Cassie transition). The contact area of the condensate tail with the nanostructures on the valley base among the four surrounding pillars is $A_{adh} = f_n \pi r_b^2$, where $r_b = \frac{W}{2} sin\theta_n$ is the radius of the tail base, $W = \sqrt{2}(1 - b)$, (Figure 1d). The surface free energy change during detachment of the tail per unit surface area would be $W_{adh} = \sigma + \sigma_{sv} - \sigma_{sl} = \sigma(1 + cos\theta)$,[22] where θ is the intrinsic contact angle on the fluoropolymer-coated (PFC 1601V, Cytonix)[11]

smooth surface. Then the energy (work of adhesion) required to detach the tail from the cavity base is

$$E_{adh} = W_{adh} \times A_{adh} = \sigma(1 + \cos\theta)f_n \pi r_b^2 \qquad (3)$$

It can be seen that the adhesion energy is reduced by a factor of f_n on the nanotextures. In this regard, Bhushan and Her studied adhesion characteristics of rose petal-inspired surfaces with hierarchical structures and they also found the pitch values of microstructures and density of nanostructures play an important role in real rose petals and artificial surfaces to control their adhesion properties.[23]

Our vapor condensation study in ESEM[11] and other moisture condensation studies[10] have observed extensive immobile coalescence on superhydrophobic surfaces, which can be ascribed to viscous dissipation and contact line friction/pinning.[17] During condensate growth in dropwise condensation, the condensate tail in the pillar cavity will finally move upwards due to either morphing-induced Laplace pressure gradient or coalescence with neighbouring droplets. To evaluate the viscous dissipation, we assumed that the Laplace pressure force F drives the condensate tail of mass m to the top portion with an eventual vertical velocity U during the expulsion process. In this study, the magnitude of viscous dissipation during the tail elevation is estimated as[24]

$$E_{vis} = \int_0^{\tau} \int_{\Omega'} \Phi d\Omega' \, dt \approx \Phi\Omega\tau \qquad (4)$$

where Ω is the volume of the condensate tail and τ is the period of viscous dissipation (In the event of coalescence, τ can be characterized as the capillary time scale[17]). In the cylindrical coordinate system (Figure 1c), the dissipation function Φ with only z direction (out of plane) movement is approximately given by

$$\Phi = 2\mu\left\{\left(\frac{\partial u_R}{\partial R}\right)^2 + \left[\frac{1}{R}\left(\frac{\partial u_\theta}{\partial \theta} + u_R\right)\right]^2 + \left(\frac{\partial u_z}{\partial z}\right)^2\right\}$$
$$+ \mu\left\{\left(\frac{\partial u_\theta}{\partial z} + \frac{1}{R}\frac{\partial u_z}{\partial \theta}\right)^2\right.$$
$$+ \left(\frac{\partial u_z}{\partial R} + \frac{\partial u_R}{\partial z}\right)^2 \qquad (5)$$
$$\left.+ \left[\frac{1}{R}\frac{\partial u_R}{\partial \theta} + R\frac{\partial}{\partial R}\left(\frac{u_\theta}{R}\right)\right]^2\right\}$$
$$\approx \mu\left(\frac{\partial u}{\partial r}\right)^2 \approx \mu\left(\frac{U/2}{W/2}\right)^2 \approx \mu\left(\frac{U}{W}\right)^2$$

In the dynamic growing process of a droplet on the pillar-arrayed surface, the surface tension σ_{LV}, the viscosity μ and the inertia govern the liquid motions. For the liquid, the ratio of viscous dissipation to surface tension and inertia is characterized by a dimensionless number, the Ohnesorge number $Oh = \mu/\sqrt{\rho\sigma_{LV}L}$, where L is the characteristic length scale (we adopt L to be the period of the pillars l), respectively. In our vapor condensation experiments, $Oh \sim 0.12$ ($\rho = 998$ kg m^{-3}, $\mu = 0.001$ Pa·s, $\sigma_{LV} = 72.8$ mN m^{-1} and $L \sim 1$ μm for the water droplet at 20° and 1 bar). Supposing the tail elevation is a capillary-inertial process ($Oh < 1$), the average velocity could be assumed to be $U/2$ and the mass center of the tail in the cavity moved upwards about $h/2$ then the time scale for the PW to Cassie transition can

be estimated as $t \sim \frac{h/2}{U/2} = \frac{h}{U}$. By the momentum law the velocity of the droplet tail could be scaled as $U^2 = \frac{Fh}{m}$.

During their evolution in condensation process, condensate droplets are usually not in a thermodynamically equilibrium state. We assumed that the expulsion of the tail is mainly due to the Laplace pressure gradient between the bottom portion and the top portion of the tail. Thus depinning of the triple line (i.e., solid-liquid-vapor contact line) occurs when a certain value of critical pressure inside a droplet is surmounted.[25] Since the tail size (pillar cavity size) is much smaller than the capillary length of 2.7 mm of water, the bottom portion of the tail is assumed to be spherical as shown in Figure 1d. So the curvature of the bottom tail can be estimated as $r_s = W/2\cos(\pi - \theta_n)$.[22] Given the larger radius of the condensate droplet on top (Figure 1c), the pressure in the top portion of the tail should be much smaller than the bottom pressure. Consequently the pressure difference in the tail can be estimated as $\Delta P = \frac{2\sigma}{r} \approx \frac{4\sigma}{W}\cos(\pi - \theta_n)$ and the vertical driving force F is scaled as

$$F \approx \frac{4\sigma}{W}\cos(\pi - \theta_n)\frac{\pi W^2}{4}$$
$$\approx \pi\sigma W \cos(\pi - \theta_n)$$
$$\approx -\pi\sigma W \cos\theta_n \qquad (6)$$

Also the mass of the tail in the cavity is approximated to be $m \approx \rho\pi W^2 h/4$, then we have $U^2 \approx \frac{-4\sigma\cos\theta_n}{\rho W}$ and the energy loss due to viscous dissipation could be estimated as

$$E_{vis} \approx \frac{1}{2}\pi\mu h^2 \sqrt{\frac{-\sigma\cos\theta_n}{\rho W}} \qquad (7)$$

CONTACT LINE DISSIPATION OF CONDENSATES ON NANOTEXTURES

From the molecular kinetic point of view[26-27] the displacement of the three-phase contact line is determined by the forward and backward liquid molecular displacement frequencies, k^+ and k^-, respectively. At equilibrium, $k^+ = k^- = k_0$, where $k_0 = \frac{k_B T}{\mu v_L}\exp(-\frac{\Delta G}{k_B T})$ is the equilibrium displacement frequency, k_B is the Boltzmann constant, T is the absolute temperature, v_L is the unit volume of flow of the liquid at the three-phase contact line and the activation free energy ΔG arises from the solid-liquid interaction, which can be taken as the work of adhesion.[28] Disturbed by external driving work (shear stress, capillary force, hydration force, van der Waals interactions, etc.), k^+ and k^- become unbalanced and the contact line will start moving. For the condensate tail in the cavity, the out-of-balance surface tension force is given by $\sigma_{sv} - \sigma_{sl} - \sigma\cos\theta_d$, where θ_d is the dynamic contact angle. When the difference between the static contact angle θ_0 and the dynamic contact angle θ_d is not significant, the contact line velocity can be linearized as $V = \frac{1}{\zeta}\gamma_{LV}(\cos\theta_0 - \cos\theta_d)$, where $\zeta = k_B T/k_0\lambda^3$ is the contact line friction coefficient that determines the dissipation rate ζV^2 within the three-phase contact zone and λ is the mean displacement distance. Both Ralston[29] and Blake[30] measured or estimated contact line friction coefficient ζ on flat hydrophobic surface and self-assembled monolayers for water and various ionic fluids respectively. For water on hydrophobic polyethylene terephthalate surface, ζ was estimated to be 0.01 Pa·s while λ is about 0.36 nm.[30] The period of the second tier CNTs on our multiscale textured surfaces is tens of nm as shown in Figure 1(b) and subsequently ζ on nanotextures can be several orders of magnitude smaller than water bulk viscosity μ of ~ 1 mPa·s, i.e., friction coefficient in the bulk, not to mention that ΔG is even smaller on textured surfaces due to surface roughness in comparison to flat surfaces. Furthermore, each condensate droplet is ideally anchored along the vertical corner edges of the four surrounding pillars, i.e., in the form of line contact as shown in Figure 1(a), consequently we assumed contact line friction dissipation is tiny compared to viscous loss on the two-tier structured surfaces.

On the other hand, we estimated contact line friction coefficient ζ by observing dropwise condensate dynamics on CNT forest via high speed CCD camera. The lateral velocity of condensate droplet of ~15 μL reached about 1 m/s with the difference between static and dynamic contact angles not in excess of 1°. Therefore contact line friction coefficient ζ on nanotextures can be even one order of magnitude smaller than water viscosity, which confirmed our ignorance of contact line friction loss in the current stage of analysis.

Combining Eqs. 3 and 7 yields the energy barrier of the PW-Cassie state transition including both the adhesion energy and the viscous dissipation

$$E_{resist} = E_{adh} + E_{vis}$$
$$= \sigma(1 + \cos\theta)f_n\pi r_b^2$$
$$+ \frac{1}{2}\pi\mu h^2\sqrt{\frac{-\sigma\cos\theta_n}{\rho W}} \qquad (8)$$

This energy barrier must be overcome by the condensate tail so as to accomplish the PW to Cassie transition, which is followed by coalescence-induced self-removal from condenser surface. We carried out parametric studies to characterize the influence of first tier pillar geometry on the energy barrier. Figure 3 shows the variation of resistant energy E_{resist} versus pillar size b while the value of solid fraction f is fixed at 0.08, i.e., < 0.1, the ad hoc standard for superhydrophobicity.[3] It can be seen in Figure 3 that for each pillar height h there exists an optimum pillar size b_m leading to a minimum resistance to state transition. Importantly, by minimizing the resistant energy, the tails of condensates formed in the cavities can transform to the Cassie state in reduced sizes during growth or after coalescence with neighbouring droplets.

The optimum pillar width b_m decreases with pillar height h so that for the first tier pillar of $1\mu m$ tall the optimum pillar width is ~$1\mu m$. Shortening pillar height leads to decreased tail volume and mass and consequently the viscous dissipation impeding the expulsion process is lowered in each cavity cell. Nevertheless pillar height cannot be arbitrarily short in engineered surface design not only for maintaining proper surface roughness but also for preventing condensate droplet sagging in to the structure cavities after PW-Cassie transition.[23] Completely wetting drops are apt to form on the fortuitous surfaces with low pillar heights

and/or large spaces between pillars. Interestingly, based on energy increasing rates analysis Liu et al. reported that micro/nano-pillars (one tier) should be in excess of 1 μm tall and have a relatively small pillar diameter and space in order for the condensed droplets to be formed in the PW state.[31]
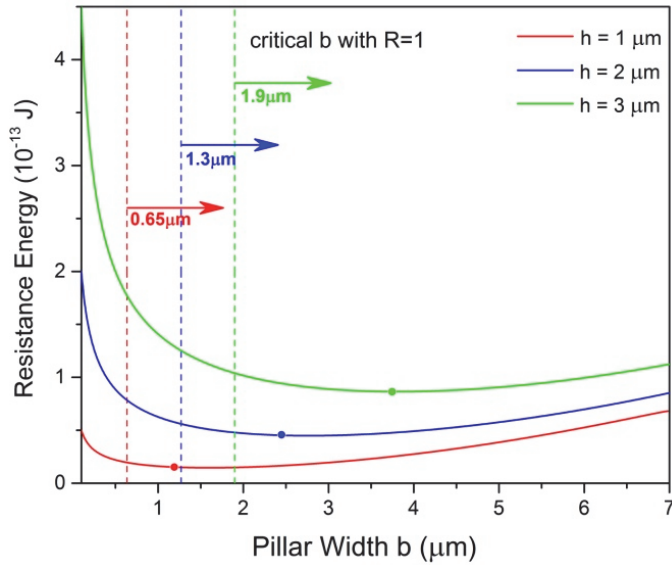

Figure 3 Resistant energy of a unit cell versus the width b of first tier pillars with $f = 0.08$. The critical pillar widths (when $R = 1$) are 0.65 μm, 1.3 μm and 1.9 μm respectively for $h = 1$ μm, 2 μm and 3 μm. Dots on each curve stand for the optimum pillar geometry b_m in each configuration.

Preferential Growth of Condensate Droplets in Cavities

On the other hand, an ideally-structured condenser surface should be able to promote out-of-plane (vertical) growth of condensate droplets formed in the surface cavities while resisting uncontrollable in-plane lateral spreading of condensates, which makes the condensates end in the Wenzel state.[32] The wider the lateral spreading within pillar cavities is, the stronger the pinning to the surface would be and consequently the less the chance of the Wenzel-Cassie transition will be. Figure 2 illustrates the condensate tail entrapped among four squarely positioned pillars. The droplet tail is outlined in frame 33″ to illustrate the anchoring role of surrounding pillars during the condensate growth. We compared surface energy change $\Delta E_{vertical}$ due to an infinitesimal vertical growth dz with surface energy change $\Delta E_{lateral}$, which is induced by an infinitesimal lateral growth dr, in term of $R = \Delta E_{vertical}/\Delta E_{lateral}$, where

$$\Delta E_{lateral} = 4\sigma[(l-b)(1-\cos\theta_n) - 2h\cos\theta_n]dr$$

$$\Delta E_{vertical} = \sigma[4(l-b) - 2\pi r_p \cos\theta_n]dz \qquad (9)$$

By equalizing the volumes required for vertical growth dz and lateral expansion dr, i.e., same condensation rate, we get

$$\frac{dz}{dr} = \frac{4(l-b)h}{[(l-b+2r_p)^2 - \pi r_p^2]} \qquad (10)$$

The energy ratio R as a function of pillar width b and first tier solid fraction f_f is plotted in Figure 4. For R values below the black plane ($R = 1$), the first tier pillars are able to block the lateral wetting of condensates in to the neighbouring cavity cells, indicative of the thermodynamically favorable configuration of surface structures. The critical pillar widths with $R = 1$ are shown in Figure 3 for various pillar heights. It can be seen that for each pillar width larger than the critical width value there does exist an optimum pillar size b_m, which not only minimizes the resistant energy but also favors vertical growth of condensates.
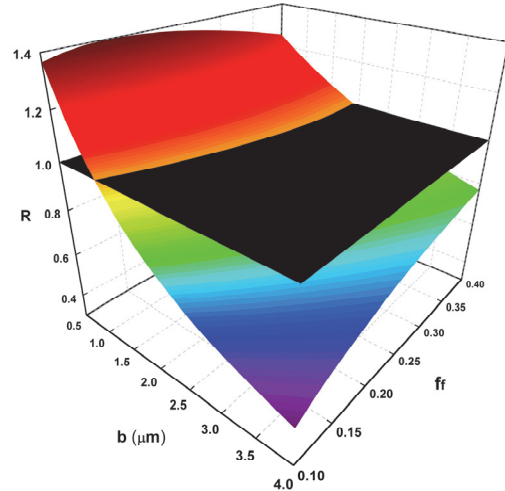

Figure 4 Change of surface energy ratio R with respect to pillar width b and first tier solid fraction f_f ($r_p = 0.2b$, $h = 3$ μm). Black plane indicates $R = 1$, below which vertical growth of condensate droplets becomes energetically favorable.

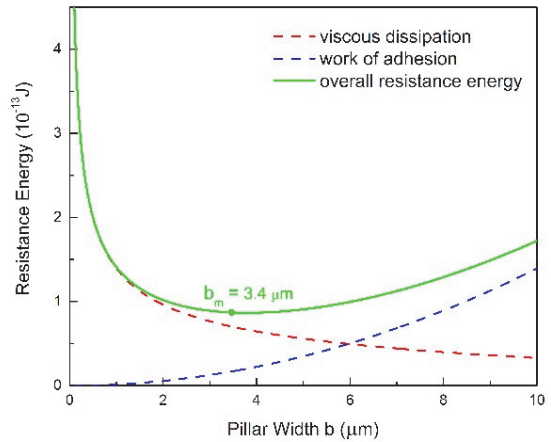**Figure 5** Variation of viscous dissipation and work of adhesion as the pillar width b changes ($f = 0.08$ and $h = 3$ μm).

We further compared viscous dissipation and work of adhesion in Figure 5 with $f = 0.08$ and $h = 3$ μm. Decreasing pillar width b has an apparent mitigating effect on work of adhesion as opposed to intensified viscous dissipation. The energy required to detach the condensate tail in the cavity increases with the increase of pillar width b (for constant pillar height h). As evidenced by the Ohnesorge number (scaled as

$Oh \sim \frac{1}{\sqrt{l}}$), viscous dissipation exhibits a different trend with the increase of the pillar gaps as indicated in Eq. 8. Indeed, there is an optimum pillar size b_m giving rise to the minimum resistant energy E_{resist}. It is noteworthy that for $b > b_m$, the dominant resistance towards PW-Cassie transition is the adhesion energy on the cavity base and for $b < b_m$ viscous dissipation plays a prominent role in resisting the condensate tail transition by dissipating more viscous energy. As confirmed in Figure 5, the pronounced increase of resistant energy for $b < b_m$ as shown in Figure 3 is due to the markedly enhanced viscous dissipation that could even prohibit the condensate tail transition.
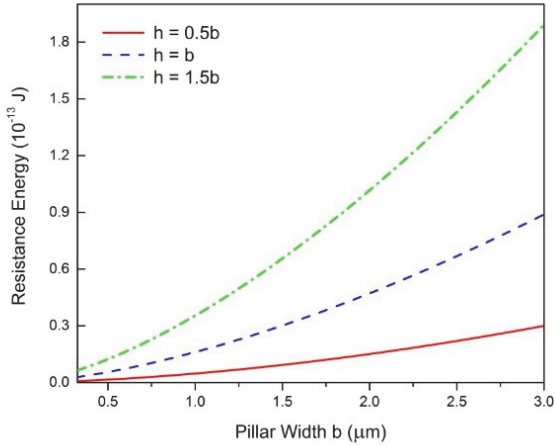

Figure 6 Resistant energy of a unit cavity cell versus first tier pillar width b for different h to b ratios ($f = 0.08$). By reducing the pillar width b the resistant energy remarkably decreases.
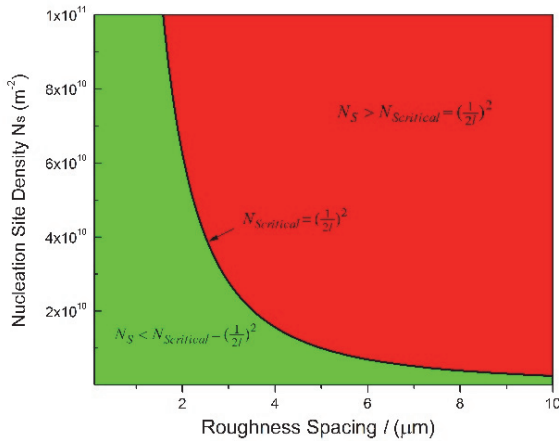

Figure 7 Critical nucleation site density $Ns_{critical}$ for different roughness spacing l.

NUCLEATION SITE DENSITY INFLUENCE ON RESISTANT ENERGY

The above analysis is subject to a constraint on the value of pillar height h, which is fixed for each configuration. While maintaining a constant solid fraction f, the pillar height h could be scaled up and down to reach a relatively lower level of resistant energy (with the optimum value b_m known). Without loss of generality, for engineered surfaces of $r_p = 0.2b$ and $f_f = 0.4$, the energy ratio R is less than 1 when $h/b < 1.57$. We selected three different h/b ratios, namely, 0.5, 1.0, and 1.5 in our analysis. Figure 6 shows the resistances towards the PW-Cassie transition of a condensate tail while the solid fraction f is held constant at 0.08. It can be seen that the resistant energy decreases monotonically with b for each fixed ratio of h/b. As the ratio of h to b grows, there is a pronounced increase of the resistance due to the enhanced viscous dissipation effect. Hence high aspect ratio pillar structures are not favored regarding self-propelled rapid removal of condensates. Figure 6 demonstrates the necessity of scaling down the first tier of hierarchical surfaces in micron or submicron scale and confirms the recent tendency to fabricate condenser surfaces with double roughness both in nanoscale.[32,33] Liu et al. used the minimum energy increasing rate (EIR) as the criterion to determine the modes of growing and wetting of condensed droplets. Consistently, through EIR analysis, they also found that by scaling down nanopillar size and pitch condensate drops are more likely to form in PW state, the ideal condensate state with enhanced heat transfer.[31]

Instead of using conventional wicks, Boreyko and Chen developed a novel vapor chamber with jumping-drop liquid return.[34] They adopted superhydrophobic condensers composed of 150–300-nm clusters of 50–100-nm silver nanoparticles and the overall (lumped) heat transfer coefficient has reached as high as 55 kW/m²·K. Similarly, Zhang et al. recently reported that superhydrophobic surfaces at steady-state do not always demonstrate superior condensation heat transfer compared to the self-assembled micro/nano silver deposited surface.[35]
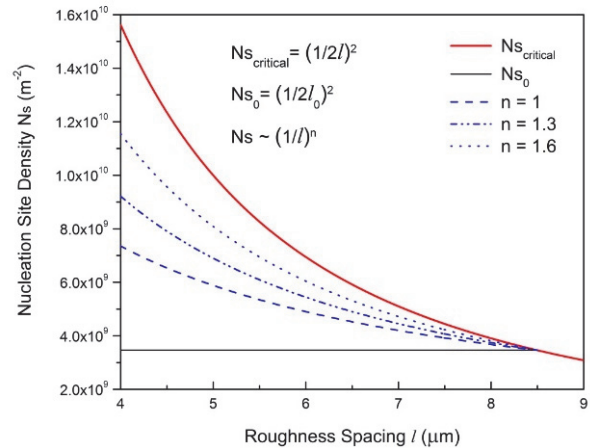

Figure 8 Different hypothetical nucleation site density Ns versus roughness spacing l.

Besides the resistant energy towards the PW-Cassie transition in a unit cavity cell, the resistant energy of the entire structured surface is necessarily demanded in order to evaluate and compare the performances of various engineered condensers. If the densities of nucleation sites are controlled to be same for various surface roughnesses, the resistant energy of

the entire surface will certainly follow the same trend for a single cavity as shown in Figure 6. Therefore by keeping the nucleation density constant, the resistant energy of the entire surface would decrease along with the pillar size b. In fact, the topography of a condenser surface has a significant influence on nucleation site density as it has been realized in numerous experimental work that nucleation sites increase consistently with the decrease of the characteristic size of microstructures on a roughness surface. Chen et al. calculated the drop number density on four types of surfaces with different microscale roughness.[36] They found that as the density of the micro-pillars increased the number of active nucleation sites grew accordingly. Lo et al. also observed an apparent increase in nucleation sites as the micro-grooves density was raised.[19] However, these works were limited to a qualitative description and there is not much theoretical work to date about the effect of multiscale surface roughness and complex degrees on nucleation site density. For condenser surfaces with different structure characteristics and length scales, the quantitative relationship between nucleation density and surface roughness should be known. Rose put forward a formula for nucleation site density as a function of minimum nucleation radius r_{min}, namely, $N_s = 0.037/r_{min}^2$, but without taking surface topography in to account.[37] By monitoring the chemical composition changes on surfaces of magnesium induced by hot condensate droplets, Mu et al. made an empirical extension of Rose's formula by only incorporating surface fractal dimension.[38] With lack of theoretical investigation on the effects of multiscale topography in heterogeneous nucleation, it is hard to quantitatively predict the relationship between roughness characteristics of an engineered surface and nucleation site density. Nevertheless the importance of controlling nucleation density in pursuit of CDC could be evidently illustrated by selecting different hypothetical nucleation densities, indicative of the influence of surface structure density on resistant energy.

Discrete nucleation sites should be methodically maintained while the uncontrolled lateral spreading should be avoided or delayed during condensate growth in pillar cavities, otherwise dropwise condensation could not continue and the surface would eventually get flooded. To satisfy this criterion the spacing between the nucleation sites L should be at least 2 times the roughness spacing l, i.e., $\frac{L}{l} > 2$.[39] The spacing between nucleation sites could be given by $L = \frac{1}{\sqrt{N_s}}$, where N_s denotes the density of nucleation sites. Then the above site criterion can be rewritten as

$$N_S \leq N_{s\,critical} = \left(\frac{1}{2l}\right)^2 \qquad (11)$$

Figure 7 shows the critical values of nucleation sites versus roughness spacing l (Eq. 11). The region beneath the critical curve (green area) represents the nucleation site densities satisfying dropwise condensation criterion mentioned above. For N_s values above the critical curve (red area) multiple nuclei may form around a unit cell. As the nuclei grow, they would merge with those in neighbouring cells leading to film condensation and may eventually flood the surface cavities. Regarding our two-tier

superhydrophobic surface[11] with $l_0 = 9\ \mu m$ and $N_{s0} = \left(\frac{1}{2l_0}\right)^2$, which works as a benchmark in this study, different nucleation densities could be selected meeting the CDC requirements as shown in Figure 8. To stay beneath the critical nucleation curve $N_{s\,critical} = \left(\frac{1}{2l}\right)^2$, the power of $\frac{1}{l}$ was chosen to be 1, 1.3, and 1.6 respectively to make Ns remain below the critical curve, i.e., in the CDC region (green zone). These nucleation density curves are hypothetically chosen in order to provide an insight into the effect of nucleation density on the overall resistant energy of surfaces of different roughness characteristics.

It can be seen in Figure 9 that for different nucleation densities the overall resistant energy of the surface displays various behaviours as the roughness size decreases. When the nucleation density is maintained at a moderate level ($n = 1$, or 1.3), the resistant energy of the surface is in proportion to the pillar width b. In contrast, as the rate of nucleation sites rises even higher ($n = 1.6$) while lowering the roughness size, the overall resistant energy of the surface could increase despite the fact that the resistant energy of a unit cell is decreasing (Figure 6). In other words the significant increase in the number of nucleation sites leads to more condensate tails in the cavities of first-tier structures. Therefore the overall resistant energy rises as a result of the increase of nucleation sites. From the experimental point of view, to maintain nucleation sites within a proper range (n < 1.6), superbiphilic surfaces formed by lithographically patterning superhydrophilic islands on superhydrophobic surfaces can be employed for spatial control of microscale droplets during condensation,[40] which is a new research theme in dropwise condensation on engineered surfaces.
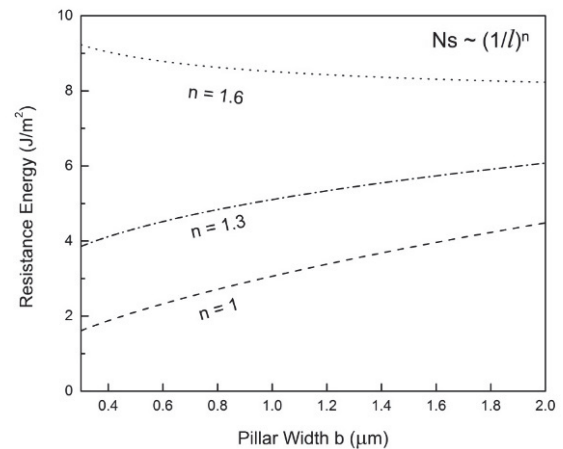

Figure 9 Resistant energy of the entire condenser surface versus first tier pillar size b for different hypothetical nucleation site densities.

CONCLUSIONS

Continued and sustained dropwise condensation on engineered surfaces places stringent requirements on careful design of surface structure length scale and geometry and

meticulous control of nucleation density, condensate morphology, and droplet departure dynamics. Condenser surfaces with hierarchical micro\nano-structures are superior to flat or solely nanostructured surfaces in controlling nucleation site density. Due to the relatively smaller energy barrier (Gibbs free energy) in the cavity of first tier structures, most of the condensate embryos/droplets in PW state can be discretely confined therein. Recent studies have found that PW-Cassie transition on engineered surfaces plays an important role in enhancing condensation heat transfer. We carried out optimization of two-tier surfaces by minimizing the resistant energy that impedes the PW-Cassie transition. Our analysis of condensate growth in a unit first tier pillar valley shows that an optimum pillar geometry does exist that can tremendously mitigate the resistant energy while allowing condensates to preferentially grow in out-of-plane direction. The second tier nanostructures play an important role in contact formation between condensed droplets and underlying substrate. We further showed that further reducing double roughness to submicron scale could be promising in achieving sustainable dropwise condensation due to even lower resistance to the PW-Cassie transition. In particular, the second tier nanotextures can effectively mitigate contact line dissipation and contact line pinning of the condensates. On the overall condenser surface, discrete nucleation sites are desired for delaying condensate flooding and superhydrophobic condenser surfaces with multiscale structures are superior to flat or solely nanotextured surfaces in controlling nucleation density. In order to further meticulously and precisely control nucleation density at elevated supersaturations, superbiphilic surfaces formed by lithographically registering superhydrophilic spots on superhydrophobic surfaces can be developed as novel condensers in order to achieve CDC. This energy-based analysis can help us design multiscale textured surfaces that can sustain CDC in strong condensation with elevated supersaturations and consequently give rise to enhanced condensation heat transfer.

REFERENCES
[1] Cassie A. B. D. and Baxter S., Wettability of porous surfaces, *Trans. Faraday Soc.,* Vol. **40**, 1944, pp. 546-551
[2] Wenzel R. N., Resistance of solid surfaces to wetting by water, *Ind. Eng. Chem.,* **Vol. 28**, 1936, pp. 988-994
[3] Miljkovic N., Enright R., Wang E. N., Effect of droplet morphology on growth dynamics and heat transfer during condensation on superhydrophobic nanostructured surfaces, *ACS Nano,* Vol. **6**, 2012, pp. 1776-1785
[4] Dorrer C. and Rühe J., Condensation and wetting transitions on microstructured ultrahydrophobic surfaces, *Langmuir,* Vol. **23**, 2007, pp. 3820-3824
[5] Enright R., Miljkovic N., Al-Obeidi A., Thompson C. V., Wang E. N., Condensation on superhydrophobic surfaces: The role of local energy barriers and structure length scale, *Langmuir,* Vol. **28**, 2012, pp. 14424-14432
[6] Liu T.-Q., Sun W., Sun X.-Y., Ai H.-R., Thermodynamic analysis of the effect of the hierarchical architecture of a superhydrophobic surface on a condensed drop state, *Langmuir,* Vol. **26**, 2010, pp. 14835-14841
[7] Miljkovic N., Enright R., Nam Y.S., Lopez K., Dou N., Sack J., Wang E. N., Jumping-droplet-enhanced condensation on scalable superhydrophobic nanostructured surfaces, *Nano Lett.,* Vol. **13**, 2013, pp. 179−187
[8] Rykaczewski K., Osborn W. A., Chinn J., Walker M. L., Scott J. H. J., Jones W., Hao C., Yao S.-H., Wang Z.-K., How nanorough is rough enough to make a surface superhydrophobic during water condensation?, *Soft Matter,* Vol **8**, 2012, pp. 8786-8794
[9] Miljkovic N., Enright R., Wang E. N., Modeling and optimization of superhydrophobic condensation, *J. Heat Transfer,* Vol. **135**, 2013, pp. 111004
[10] Chen C.-H., Cai Q.-J., Tsai C.-L., Chen C.-L., Xiong G.-Y., Yu Y., Ren Z.-F., Dropwise condensation on superhydrophobic surfaces with two-tier roughness, *Appl. Phys. Lett.,* Vol. **90**, 2007, pp. 173108
[11] Cheng J.-T., Vandadi A., Chen C.-L., Condensation heat transfer on two-tier superhydrophobic surfaces, *Appl. Phys. Lett.,* Vol. **101**, 2012, pp. 131909
[12] Boreyko J. B., Chen C.-H., Self-propelled dropwise condensate on superhydrophobic surfaces., *Phys. Rev. Lett.,* Vol **103**, 2009, pp. 184501
[13] Jung Y. C. and Bhushan B., Wetting transition of water droplets on superhydrophobic patterned surfaces, *Scripta Materialia,* Vol. **57**, 2007, pp. 1057-1060
[14] Narhe R. D. and Beysens D. A., Growth dynamics of water drops on a square-pattern rough hydrophobic surface., *Langmuir,* Vol. **23**, 2007, pp. 6486-6489
[15] Sbragaglia M., Peters A. M., Pirat C., Borkent B. M., Lammertink R. G. H., Wessling M., Lohse D., Spontaneous breakdown of superhydrophobicity, *Phys. Rev. Lett,* Vol. **99**, 2007, pp. 156001
[16] Patankar N. A., Transition between superhydrophobic states on rough surfaces, *Langmuir,* Vol. **20**, 2004, pp. 7097-7102
[17] Wang F.-C., Yang F.-Q., Zhao Y.-P., Size effect on the coalescence-induced self-propelled droplet., *Appl. Phys. Lett.,* Vol. **98**, 2011, pp. 053112
[18] Carey V.P., Liquid-Vapor Phase-Change Phenomena: An Introduction to the Thermophysics of Vaporization and Condensation Processes in Heat Transfer Equipment, Taylor & Francis Group, 2008
[19] Lo C.-W., Wang C.-C., Lu M.-C, Spatial control of heterogeneous nucleation on the superhydrophobic nanowire array, *Adv. Funct. Mater.,* Vol. **24**, 2014, pp. 1211-1217
[20] Bahadur V. and Garimella S. V., Electrowetting-based control of static droplet states on rough surfaces, *Langmuir,* Vol. **23**, 2007, pp. 4918-4924
[21] Bahadur V. and Garimella S. V., Electrowetting-based control of droplet transitions and morphology on artificially microstructured surfaces, *Langmuir,* Vol. **24**, 2008, pp. 8338-8345
[22] De Gennes P.-G., Brochard-Wyart F., Quéré D., Capillarity and wetting phenomena: drops, bubbles, pearls, waves, Springer, 2004
[23] Bhushan B. and Her E. K, Fabrication of superhydrophobic surfaces with high and low adhesion inspired from rose petal, *Langmuir,* Vol. **26**, 2010, pp. 8207-8217

[24] Chandra S. and Avedisian C. T., On the collision of a droplet with a solid surface, *Proc. R. Soc. Lond. A,* Vol. **432**, 1991, pp. 13-41

[25] Whyman G. and Bormashenko E., How to make the Cassie wetting state stable?, *Langmuir,* Vol. **27**, 2011, pp. 8171–8176

[26] Blake T. D., The physics of moving wetting lines., *J. Colloid Interface Sci.,* 2006, **Vol. 299**, 2006, pp. 1-13

[27] Snoeijer J. H. and Andreotti B., Moving contact lines: scales, regimes, and dynamical transitions., *Annu. Rev. Fluid Mech.*, Vol. **45**, 2013, pp. 269-292

[28] Yuan Q.-Z., Huang X.-F., Zhao Y.-P., Dynamic spreading on pillar-arrayed surfaces: viscous resistance versus molecular friction, *Physics Fluids,* Vol. **26**, 2014, pp. 092104

[29] Li H., Paneru M., Sedev R., Ralston J., Dynamic electrowetting and dewetting of ionic liquids at a hydrophobic solid–liquid interface, *Langmuir,* Vol. **29**, 2013, pp. 2631−2639

[30] Vou M., Rioboo R., Adao M. H., Conti J., Bondar A. I., Ivanov D. A., Blake T. D., Coninck J. De., Contact-line friction of liquid drops on self-assembled monolayers: chain-length effects, *Langmuir,* Vol. **23**, 2007, pp. 4695-4699

[31] Liu T.-Q., Sun W., Li X.-Q., Sun X.-Y., Ai H.-R., Growth modes of condensates on nano-textured surfaces and mechanism of partially wetted droplet formation, *Soft Matter,* Vol. **9**, 2013, pp. 9807-9815

[32] Larmour I. A., Bell S. E. J., Saunders G. C., Remarkably simple fabrication of superhydrophobic surfaces using electroless galvanic deposition, *Angewandte Chemie,* Vol. **119**, 2007, 1740-1742

[33] He M., Zhou X., Zeng X.-P., Cui D.-P., Zhang Q.-L., Chen J., Li H.-L., Wang J.-J., Cao Z.-X., Song Y.-L., Jiang L., Hierarchically structured porous aluminum surfaces for high-efficient removal of condensed water, *Soft Matter,* Vol. **8**, 2012, pp. 6680-6683

[34] Boreyko J. B. and Chen C.-H., Vapor chambers with jumping-drop liquid return from superhydrophobic condensers, *Int. J. Heat Mass Transfer,* Vol. **61**, 2013, pp. 409-418

[35] Zhang B.-J., Kuok C., Kim K. J., Hwang T., Yoon H. K., Dropwise steam condensation on various hydrophobic surfaces: Polyphenylene sulfide (PPS), polytetrafluoroethylene (PTFE), and self-assembled micro/nano silver (SAMS), *Int. J. Heat Mass Transfer,* Vol. **89**, 2015, pp. 353–358

[36] Chen X.-M., Wu J., Ma R.-Y., Hua M., Koratkar N., Yao S.-H., Wang Z.-K., Nanograssed micropyramidal architectures for continuous dropwise condensation, *Adv. Funct. Mater.,* **21**, 2011, 4617-4623

[37] Rose J. W., Dropwise condensation theory and experiment: a review, *Proc Instn Mech Engrs Part A: J Power and Energy,* Vol. **216**, 2002, pp. 115-128

[38] Mu C.-F., Pang J.-J., Lu Q.-Y., Liu T.-Q., Effects of surface topography of material on nucleation site density of dropwise condensation, *Chem. Eng. Sci.,* Vol. **63**, 2008, pp. 874-880

[39] Miljkovic N. and Wang E. N., Condensation heat transfer on superhydrophobic surfaces, *MRS Bulletin,* Vol. **38**, 2013, pp. 397-406

[40] Ölçeroğlu E. and McCarthy M., Spatial control of condensate droplets on superhydrophobic surfaces, *J. Heat Transfer,* Vol. **137**, 2015, pp. 080905-1